Chaotic spiking and incomplete homoclinic scenarios in semiconductor lasers with optoelectronic feedback

2009 New J. Phys. 11 073022

(http://iopscience.iop.org/1367-2630/11/7/073022)

New Journal of Physics
The open-access journal for physics

Chaotic spiking and incomplete homoclinic scenarios in semiconductor lasers with optoelectronic feedback

Kais Al-Naimee[1,2], Francesco Marino[3], Marzena Ciszak[1], Riccardo Meucci[1] and F Tito Arecchi[1,3]

[1] CNR-Istituto Nazionale di Ottica Applicata, Largo E Fermi 6, 50125 Firenze, Italy
[2] Physics Department, College of Science, University of Baghdad, Baghdad, Iraq
[3] Dipartimento di Fisica, Università di Firenze, INFN, Sezione di Firenze, Via Sansone 1, I-50019 Sesto Fiorentino (FI), Italy
E-mail: marzena.ciszak@inoa.it

New Journal of Physics **11** (2009) 073022 (11pp)
Received 16 March 2009
Published 9 July 2009
Online at http://www.njp.org/
doi:10.1088/1367-2630/11/7/073022

Abstract. We demonstrate experimentally and theoretically the existence of slow chaotic spiking sequences in the dynamics of a semiconductor laser with ac-coupled optoelectronic feedback. The timescale of these dynamics is fully determined by the high-pass filter in the feedback loop and their erratic, though deterministic, nature is evidenced by means of the interspike interval (ISI) probability distribution. We eventually show that this regime is the result of an incomplete homoclinic scenario to a saddle-focus, where an exact homoclinic connection does not occur.

Contents

1. Introduction

Irregular spiking sequences in biological, chemical and electronic systems have been frequently observed to be the result of multiple timescale dynamics [1]. Indeed, a variety of natural systems showing this behavior (neural cells [2], cardiac tissues [3], chemical reactions [4], to name just a few) can be mathematically described by means of slow and fast variables coupled together (slow–fast systems). In two-dimensional phase spaces irregular spiking can forcibly appear only in the presence of noise close to fixed points/limit cycles bifurcations (Andronov saddle-node collisions, sub and super critical Hopf bifurcations, etc). In contrast, higher dimensional systems can support more varied and complex dynamics, such as mixed-mode oscillations [5, 6] and erratic bursting [2]. Here, irregular spikes are the result of complicated bifurcation sequences, thus having a purely deterministic origin (chaotic spiking).

In many cases [7]–[10] these phenomena can be understood in terms of a paradigmatic model known as Shilnikov homoclinic chaos (HC) [11]. HC may arise in three-dimensional phase space when a growing periodic orbit approaches a saddle-focus becoming homoclinic to it, i.e. biasymptotic for $t \to \pm\infty$. Typical time series consist of large pulses (associated with a homoclinic orbit in the phase space) separated by irregular time intervals in which the system displays small-amplitude chaotic oscillations. This behavior arises in agreement with the Shilnikov theorem, which predicts the occurrence of complex dynamics near homoclinicity whenever the saddle-focus, with linearized eigenvalues $(\mu, -\rho \pm \mathrm{i}\omega)$, $(\rho, \mu > 0)$, satisfies the condition $|\rho/\mu| < 1$.

However, the original Shilnikov scenario is not a general explanation for the appearance of chaotic spiking. Although each spike is obviously associated with some reinjection mechanism, it is clear that there is no reason for such a reinjection to occur through a homoclinic orbit. For instance, and in particular in slow–fast systems, a Hopf bifurcation can be followed by a period doubling cascade producing a sequence of small-periodic and chaotic excitable attractors, that develops before relaxation oscillations arise. As the mean amplitude of the chaotic attractors grows, some fluctuations of the chaotic background spontaneously trigger excitable spikes in an erratic but deterministic sequence [12]. Such phenomena are often referred to as *incomplete* homoclinic scenarios [13] since, in the appropriate parameter range, they may *mimic* trajectories close to Shilnikov conditions.

In order to understand these complex dynamics, frequently observed in biological environments, and to provide controllable and reproducible experiments, considerable efforts have been devoted to the search for analogous phenomena in nonlinear optical systems, and HC has been found in CO_2 lasers with feedback [14] and with a saturable absorber [15].

However, in view of future experiments concerning synchronization in laser arrays, semiconductor lasers appear to be ideal candidates since they allow the realization of a miniaturized chip of optoelectronically coupled units. To this end, the aim of this work is to study the occurrence of chaotic spiking in a semiconductor laser with ac-coupled nonlinear optoelectronic feedback. The solitary laser dynamics is ruled by two coupled variables (intensity and population inversion) evolving with two very different characteristic timescales. The introduction of a third degree of freedom (and a third timescale) describing the ac-feedback loop, leads to a three-dimensional slow–fast system displaying a transition from a stable steady state to periodic spiking sequences as the dc-pumping current is varied. For intermediate values of the current, a regime is found where regular large pulses are separated by fluctuating time intervals in a scenario resembling HC. The timescale of these dynamics, much slower with

respect to typical semiconductor laser timescales (few ns), is fully determined by the high-pass filter in the feedback loop. We eventually provide a minimal physical model reproducing qualitatively the experimental results and showing that chaotic spiking is the consequence of an incomplete homoclinic scenario to a saddle-focus, where an exact homoclinic connection does not occur.

2. Experiment

We consider a closed-loop optical system, consisting of a single-mode semiconductor laser with ac-coupled nonlinear optoelectronic feedback. The output laser light is sent to a photodetector producing a current proportional to the optical intensity. The corresponding signal is sent to a variable gain amplifier characterized by a nonlinear transfer function of the form $f(w) = Aw/(1+sw)$, where A is the amplifier gain and s a saturation coefficient, and then fed back to the injection current of the laser. The feedback strength is determined by the amplifier gain, while its high-pass frequency cutoff can be varied (between 1 Hz and 100 kHz) by means of a tunable high-pass filter. The laser (Mitsubishi ML925B6F) consists of a InGaAsP-multiple quantum well Fabry–Perot laser diode, which provides a stable single transverse-mode oscillation with emission wavelength of 1550 nm and continuous light output of 5 mW. The pumping current is set close to the solitary laser threshold value (8.3 mA) and the net gain of the whole feedback loop has been fixed to 10. Fixing both the feedback gain and frequency cutoff and increasing the dc-pumping current, we observe the dynamical sequence shown in figures 1(a)–(c). In the upper panel, corresponding to the lowest current, the detected optical power is stable. As the current is delicately increased a transition to a chaotically spiking regime is observed, where large intensity pulses are separated by irregular time intervals in which the system displays small-amplitude chaotic oscillations (figure 1(b)). This scenario is qualitatively similar to HC as evidenced by the characteristic time series and the experimental reconstruction of the phase portrait through the Ruelle–Takens embedding technique (figure 1(d)). Further increase of the current makes the firing rate higher until a periodic regime is eventually reached (figure 1(c)). In correspondence to the large pulses, each oscillation period can be decomposed into a sequence of periods of slow motion, near extrema, separated by fast relaxations between them. This behavior (relaxation oscillations) is typical of slow–fast systems. A similar dynamical sequence can be obtained as the pumping current is kept constant and the amplifier gain is changed.

As in HC, the pulse duration (associated with a precise orbit in the phase space) is uniform, while the interpulse times vary irregularly. This is shown by the corresponding interspike interval (ISI) probability distribution (figure 1(e)) consisting of an exponentially decaying function of time, typical of random processes, displaced by the pulse duration, acting as a refractory time. Such a distribution is reminiscent of the one observed in noisy excitable systems, where the system responds by randomly spiking on a noisy background [16]. Here, however, there are no external forces, and the small chaotic background is clearly larger than the residual electronic noise. Moreover, the ISI histogram displays a structure of sharp peaks (indicated by the arrow in figure 1(e)) that could correspond to unstable periodic orbits embedded in the chaotic attractor [12]. Indeed, we will show in the last section that a similar distribution can be obtained by a fully deterministic model of our experiment.

The complete dynamics in our system is ruled by two coupled variables (intensity and population inversion) evolving with two very different characteristic timescales.

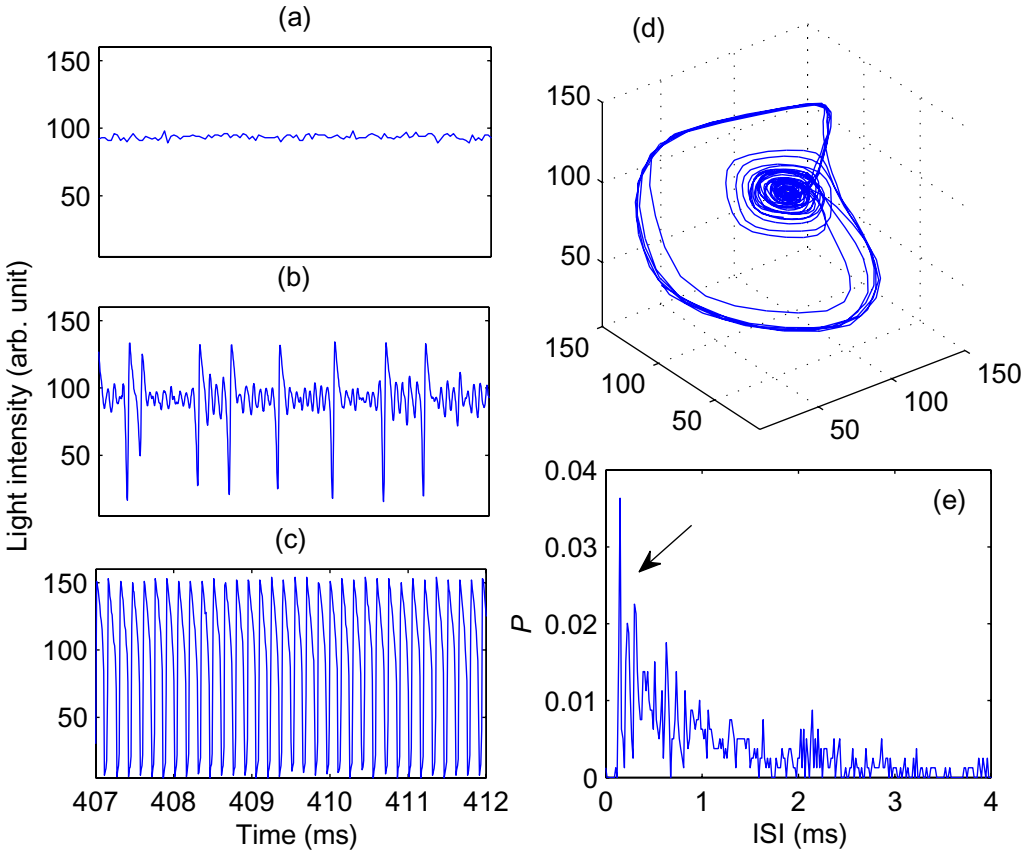

Figure 1. Transition from a stationary steady state to chaotic spiking and eventually periodic self-oscillations as the dc-pumping current is varied. (a) 8.700 mA, (b) 8.763 mA and (c) 9.050 mA. The net feedback-loop gain is 10, and is kept fixed. (d) Experimental reconstruction of the phase portrait through the Ruelle–Takens embedding technique. (e) The corresponding experimental ISI probability distribution for the chaotic spiking regime.

The introduction of an ac-feedback optoelectronic loop adds both a third degree of freedom and a third much slower timescale. While the former timescales cannot be varied experimentally and therefore their effects on the system dynamics cannot be easily displayed, the latter one can be changed by adjusting the high-pass frequency in the feedback loop. Results are reported in figure 2 where the time series in the chaotic spiking regime has been compared for different values of the feedback cutoff frequency. It is immediately evident that the increase of the cutoff frequency leads to faster chaotic spiking regimes (figures 2(a)–(c)) until that the characteristic slow–fast pulses disappear and only a fast large-amplitude chaos remains (figure 2(d)). As we will discuss later, this occurs when the timescale split becomes too small to support slow–fast pulses.

3. Dynamical model

The dynamics of the photon density S and carrier density N is described by the usual single-mode semiconductor laser rate equations [17] appropriately modified in order to include the

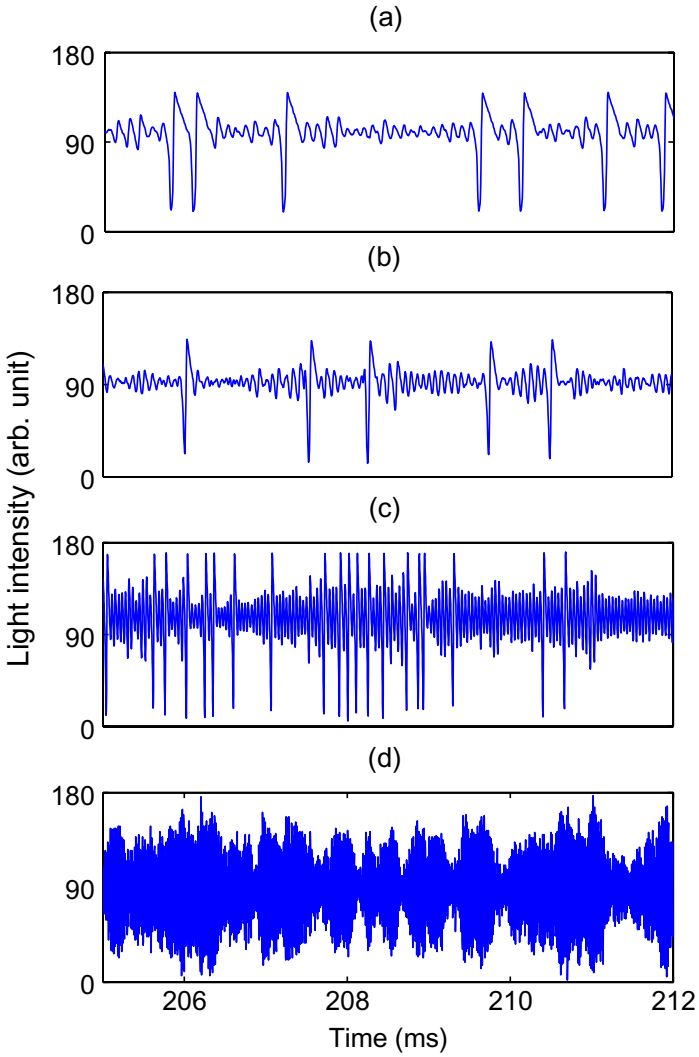

Figure 2. Chaotic spiking regime for different values of the feedback cutoff frequency. (a) 0.1 kHz, (b) 0.25 kHz, (c) 1 kHz and (d) 5 kHz. Dc-pumping current is 8.727 mA.

ac-coupled feedback loop

$$\dot{S} = \left[g(N - N_{\mathrm{t}}) - \gamma_0\right] S, \quad \dot{N} = \frac{I_0 + f_{\mathrm{F}}(I)}{eV} - \gamma_c N - g(N - N_{\mathrm{t}})S, \quad \dot{I} = -\gamma_{\mathrm{f}} I + k\dot{S}, \tag{1}$$

where I is the high-pass-filtered feedback current (before the nonlinear amplifier), $f_{\mathrm{F}}(I) \equiv AI/(1 + s'I)$ is the feedback amplifier function, I_0 is the bias current, e the electron charge, V is the active layer volume, g is the differential gain, N_{t} is the carrier density at transparency, γ_0 and γ_{c} are the photon damping and population relaxation rate, respectively, γ_{f} is the cutoff frequency of the high-pass filter and k is a coefficient proportional to the photodetector responsivity. Compared with optical feedback, optoelectronic feedback is reliable and robust because the system is insensitive to optical phase variations [18]–[20]. For this reason the phase dynamics of the optical field can be eliminated. A detailed physical model of the experimental system should also include a series of low-pass frequency filters arising from the limited bandwidth of the

photodiode, the electrical connections to the laser, parasite capacitances, and other undesirable electronic effects. However, we will see that such additional filters do not play a critical role in a qualitative description of the observed dynamics, which is the aim of the present model.

For numerical and analytical purposes, it is useful to rewrite equations (1) in dimensionless form. To this end, we introduce the new variables $x = \frac{g}{\gamma_c} S$, $y = \frac{g}{\gamma_0}(N - N_t)$, $w = \frac{g}{k\gamma_c} I - x$ and the timescale $t' = \gamma_0 t$. The rate equations then become

$$\dot{x} = x(y-1), \tag{2}$$

$$\dot{y} = \gamma(\delta_0 - y + f(w+x) - xy), \tag{3}$$

$$\dot{w} = -\epsilon(w+x), \tag{4}$$

where $f(w+x) \equiv \alpha \frac{w+x}{1+s(w+x)}$, $\delta_0 = (I_0 - I_t)/(I_{th} - I_t)$, ($I_{th} = eV\gamma_c(\frac{\gamma_0}{g} + N_t)$ is the solitary laser threshold current), $\gamma = \gamma_c/\gamma_0$, $\varepsilon = \omega_0/\gamma_0$, $\alpha = Ak/(eV\gamma_0)$ and $s = \gamma_c s' k/g$.

4. Geometric theory of singular perturbation

The blow up of large slow–fast phase-space orbits and the occurrence of a chaotic spiking regime can be understood through the following qualitative analysis. All the parameters appearing in equations (2)–(4) are $\mathcal{O}(1)$ quantities except the ratio of the photon lifetimes to the carrier lifetime, γ which is of the order of 10^{-3}, and the renormalized cutoff frequency, typically much smaller than γ. In these conditions equations (2)–(4) become a singularly perturbed system of three timescales, with the rates of change for the dimensionless intensity, carriers and feedback current ranging from fast to intermediate to slow, respectively. Geometric theory of singular perturbation thus is readily applicable [21]. Since w typically changes at a much slower rate than x and y, the motion splits into fast and slow epochs [22]. During the fast evolution, the change of w can be neglected and the dynamics be described by equations (2) and (3) with $w = \text{const}$ as a parameter. The 'fixed points' of this dynamical subsystem lay on the one-dimensional manifold $\Sigma = \Sigma_x \cup \Sigma_y$ where Σ_x is given by the trivial nullcline $\{(x = 0, y_w = \delta_0 + f(w), w)\}$ and $\Sigma_y = \{(x_w, y = 1, w)\}$ is defined by the equation $\delta_0 + f(x_w + w) - 1 - x_w = 0$. It is on this manifold then, where the slow dynamics described by equation (4) can now take place. With respect to the fast dynamics (2) and (3) defined on the planes $w = \text{const}$ transversal to the slow manifold, the fixed points along Σ_y are saddles if $f'(x_w + w) > 1$ (here f' is the derivative of f with respect to the x variable), stable foci if $f'(x_w + w) < 1 - \gamma(1 + x_w)^2/4x_w$ and stable nodes in the small γ-wide band of phase space, where $1 - \gamma(1 + x_w)^2/4x_w < f'(x_w + w) < 1$. On Σ_x, we have stable nodes if $f(w) < 1 - \delta_0$ and saddles if $f(w) > 1 - \delta_0$, where the point given by $f(w) = 1 - \delta_0$ is the intersection between the curves defined by Σ_x and Σ_y. Therefore, the slow manifold Σ is composed of two attracting branches (solid curves in figure 3) $\Sigma_1 = \Sigma_x \cap \{f'(x_w + w) < 1\}$ and $\Sigma_2 = \Sigma_x \cap \{f(w) < 1 - \delta_0\}$ separated by a repelling branch, $\Sigma_3 = \Sigma_y \cap \{f'(x_w + w) > 1\}$, and a further repelling branch $\Sigma_4 = \Sigma_x \cap \{f(w) > 1 - \delta_0\}$ (repelling branches are dashed lines in figure 3).

Now let w slowly vary accordingly to equation (4). Since the branches $\Sigma_{1,2}$ rapidly attract all neighboring trajectories—while $\Sigma_{3,4}$ repel them—most of the time the motion has to take place along these branches. There, equation (4) dictates that w decreases for $w > -x_w$ (shaded region in figure 3) and grows for $w < -x_w$. Whenever this prescription forces the system to reach the turning point $f'(x_w + w) = 1$ on Σ_y, the trajectory forcibly jumps to Σ_2 and flows

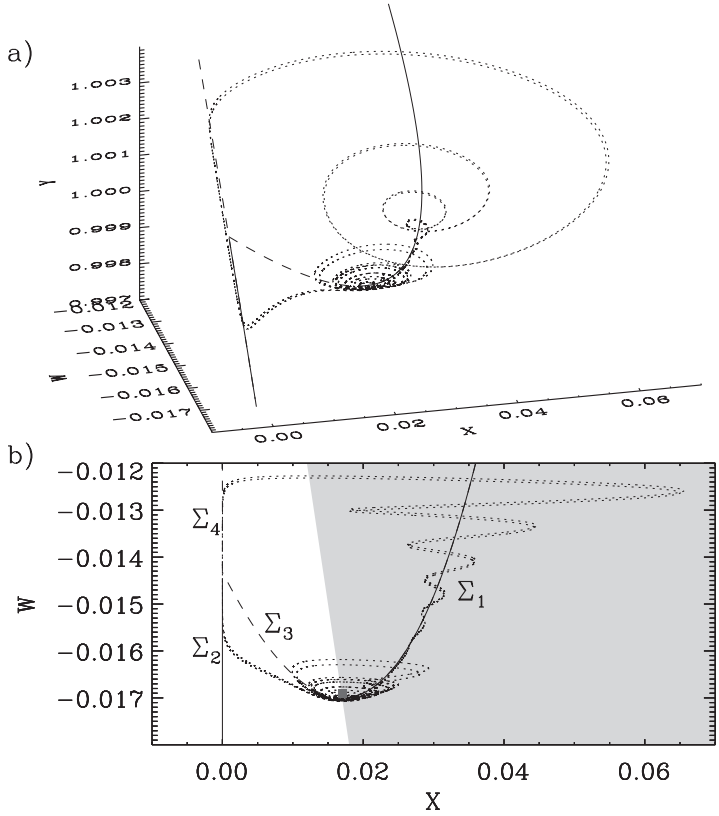

Figure 3. (a) Slow manifold of the system (2–4) with a typical chaotic trajectory (dotted line) and (b) their projection on the (w, x) plane. Solid and dashed lines indicate the attracting and repelling parts of the slow manifold, respectively. The shaded area indicates the region where $w > -x$. The full square is the fixed point of the complete system (x_1, y_1, z_1). Parameters are $s = 11$, $\alpha = 1$, $\gamma = 10^{-3}$, $\epsilon = 2 \times 10^{-5}$ and $\delta_0 = 1.017$.

along this branch. Then, when the repelling part Σ_4 is reached, the trajectory will jump back (after a certain amount of time) to Σ_1. Since, apart from a small region around the turning point, Σ_1 consists of stable foci of the fast subsystem, the trajectories near—but not strictly on—this branch are shrinking helicoids. This is particularly evident immediately after the jump, as shown in figure 3. Such helicoidal trajectories physically correspond to laser relaxation oscillations, which are frequency filtered by our detection system. We conclude this analysis remarking the key differences between the present case and homoclinic orbits. The timescale separation makes the flow pass very close to the saddle-focus (x_1, y_1, z_1), thus resembling a homoclinic trajectory. However, since (x_1, y_1, z_1) is located precisely on the slow manifold (square point in figure 3(b)), the exact homoclinic connection does not occur.

5. Numerical results and discussion

The chaotic spiking regime arises from the interplay of the large phase-space orbits mentioned before and a period doubling route to chaos occurring in the vicinity of the turning point.

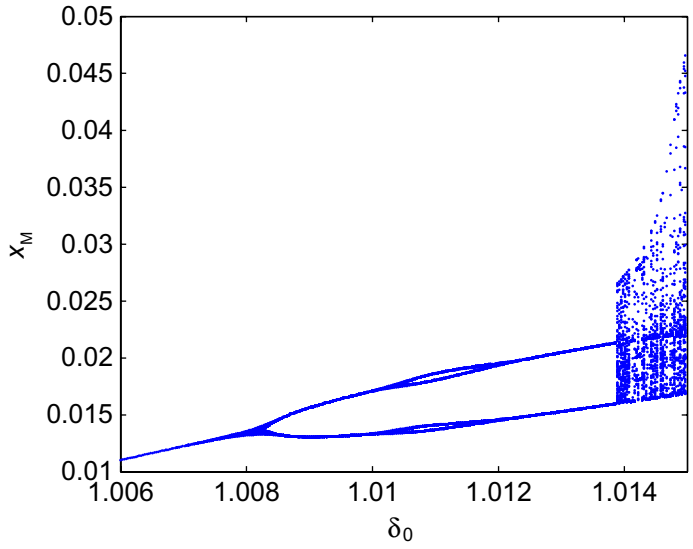

Figure 4. Bifurcation diagram for the peak values of x as the parameter δ_0 is varied. Other parameters as in figure 3.

In correspondence with the laser threshold, $\delta_0 = 1$, the system undergoes a transcritical bifurcation where the zero intensity solution, $(x_0, y_0, z_0) = (0, \delta_0, 0)$ and the lasing solution $(x_1, y_1, z_1) = (\delta_0 - 1, 1, 1 - \delta_0)$ become unstable and stable, respectively. Above the threshold, the stationary lasing solution loses stability through a supercritical Hopf bifurcation. This occurs when $\delta_0 = \delta_H$, defined by the equation

$$\gamma(\varepsilon - \alpha + 1)\delta_H^2 + (\gamma(\alpha - 1) + \varepsilon(\varepsilon - \alpha))\delta_H + \varepsilon\alpha = 0, \tag{5}$$

where a zero-amplitude harmonic limit cycle of angular frequency $\Omega = \sqrt{\frac{\gamma\varepsilon(\delta_H - 1)}{(\gamma\delta_H + \varepsilon)}}$ starts to grow. Between this bifurcation and the periodic spiking the system passes through a cascade of period doubled and chaotic attractors of small amplitude. This is illustrated by figure 4 where a bifurcation diagram is computed from our system by varying δ_0 over a small interval contiguous to the initial Hopf bifurcation. As δ_0 approaches the turning point $f'(x_w + w) = 1$, the mean amplitude of the attractors grows, until the chaotic fluctuations are sufficiently large to eventually trigger the fast dynamics. This results in an erratic—sensitive to initial conditions—sequence of homoclinic-like spikes on top of a chaotic background (figure 5(a)). The corresponding ISI histogram (figure 5(b)) shows that the aperiodic (chaotic) background triggers the (excitable) spikes in an erratic sequence, as indicated by its exponential tails. However, on top of this background the ISI histogram displays a complicated structure of sharp peaks revealing the complex structure of unstable periodic orbits embedded in the chaotic attractor nonlinearly filtered by the excitability threshold.

We have eventually studied the chaotic spiking dynamics as the parameter ϵ (corresponding to the high-pass frequency in the feedback loop) is increased. As in the experiment, the increase of the cutoff frequency leads to faster chaotic spiking regimes until the duration of the slow–fast pulses becomes of the order of the chaotic background characteristic timescale (figure 6). On the basis of the analysis in the previous paragraph, it is now clear that the period of the phase-space orbit is fully determined by the timescale split between the faster semiconductor laser timescales and the much slower timescale of the ac-feedback loop. When the feedback cutoff increases such

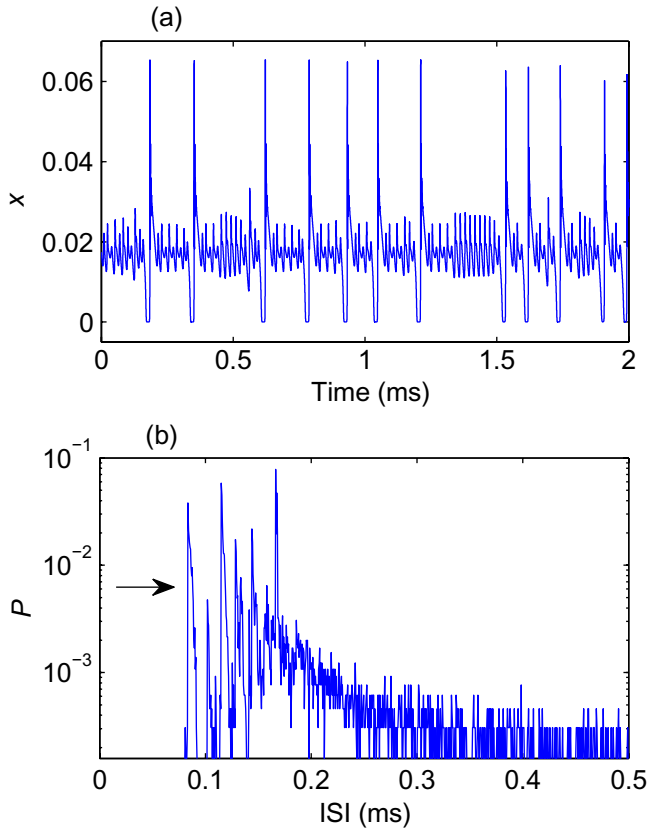

Figure 5. (a) Chaotically spiking regime and (b) the corresponding numerical ISI distribution. Parameters as in figure 3.

split decreases until it becomes too small to support slow–fast relaxation oscillations. In these conditions, geometric theory of singular perturbation no longer applies and the small-amplitude chaotic attractor grows without spikes.

We now can notice a further difference between the present case and homoclinic scenarios. While in the case of HC the small-amplitude chaotic oscillations take place in the plane of the slow manifold, here they occur in the fold of the slow manifold, i.e. in a plane transverse to the slow manifold itself [13]. This fact, together with the missing homoclinic connection mentioned before, are the signatures of incomplete homoclinic scenarios.

In conclusion, we demonstrate experimentally the existence of slow chaotic spiking sequences in the dynamics of a semiconductor laser with ac-coupled optoelectronic feedback. The timescale of these dynamics is fully determined by the high-pass filter in the feedback loop and their erratic, though deterministic, nature is evidenced by means of the ISI probability distribution. We eventually provided a feasible minimal model reproducing qualitatively the experimental results and allowing an interpretation in terms of an incomplete homoclinic scenario to a saddle-focus, where an exact homoclinic connection does not occur.

In order to improve the quantitative agreement between theory and experiments several modifications of the rate equations can be proposed, taking into account intrinsically quantum effects such as spontaneous emission, fast saturable absorption and Auger recombination. These effects usually appear in the equations in the form of additive nonlinear terms, multiplied by

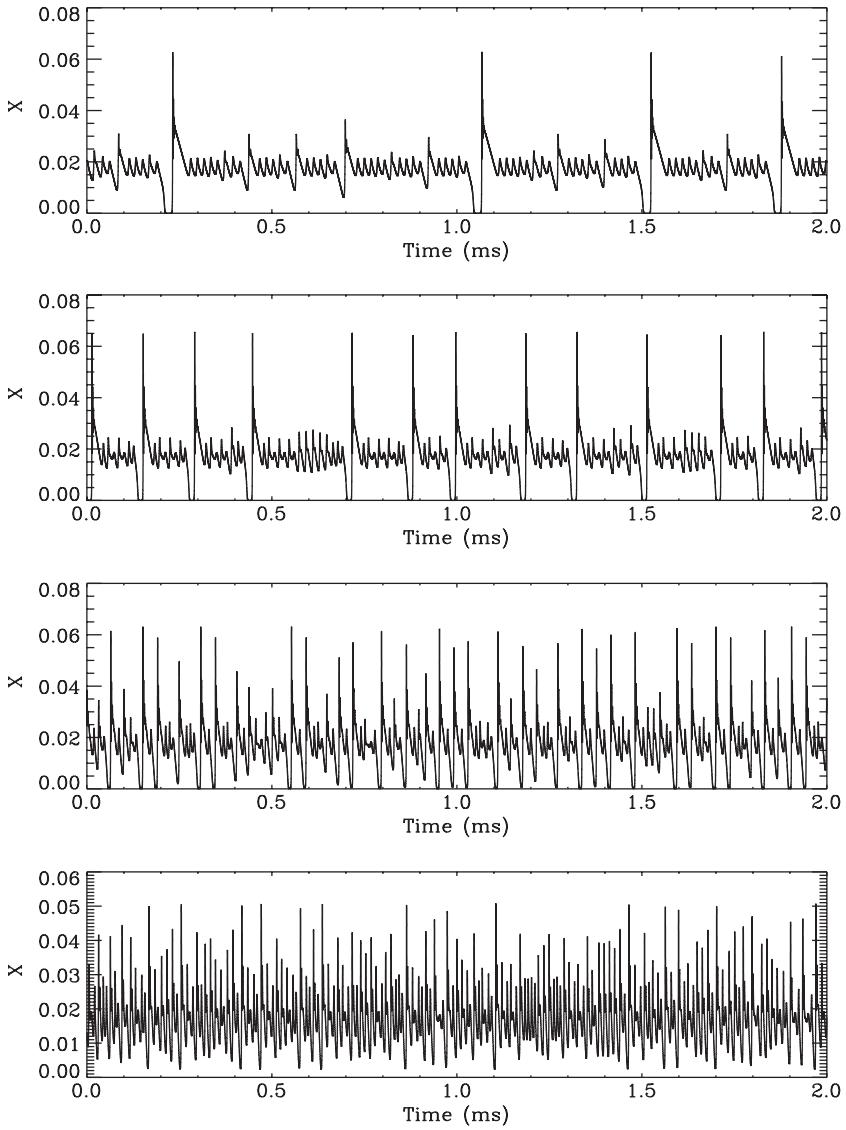

Figure 6. Chaotic spiking regime for different values of the parameter ϵ: (a) 9×10^{-6}, (b) 2×10^{-5}, (c) 4×10^{-5} and (d) 8×10^{-5}. Other parameters as in figure 3.

(usually very small) coefficients. Therefore, it is expected that they should not imply strong modifications of the slow-manifold shape which, as discussed above, is responsible for the observed dynamics.

Experiments concerning synchronization phenomena in laser arrays are currently in preparation and will be the subject of future work.

Acknowledgments

KAl-N acknowledges the ICTP–TRIL program and Landau Network, Centro Volta, Como for financial support. MC acknowledges the Marie Curie European Reintegration Grant within

the 7th European Community Framework Programme. Work partly supported by the contract 'Dinamiche cerebrali caotiche' of Ente Cassa di Risparmio di Firenze.

References

[1] Jones C K and Khibnik A I 2000 *Multiple-Time-Scale Dynamic Systems* (*IMA Proc.* vol 122) (New York: Springer)
[2] Izhikevich E 2000 *Int. J. Bifurcation Chaos* **10** 1171
[3] Davidenko J M, Pertsov A V, Salomonsz R, Baxter W and Jalife J 1992 *Nature* **355** 349
[4] Zhabotinskii A M 1974 *Concentration Autooscillations* (Moscow: Nauka)
[5] Albahadily F N, Ringland J and Schell M 1989 *J. Chem. Phys.* **90** 813
[6] Petrov V, Scott S K and Showalter K 1992 *J. Chem. Phys.* **97** 6191
[7] Vidal C 1981 *Chaos and Order in Nature* ed H Haken (Berlin: Springer) p 69
[8] Elezgaray J and Arneodo A 1992 *Phys. Rev. Lett.* **68** 714
[9] Braun T, Lisboa J A and Gallas J A C 1992 *Phys. Rev. Lett.* **68** 2770
[10] Saparin P I, Zaks M A, Kurths J, Voss A and Anishchenko V S 1996 *Phys. Rev. Lett.* **54** 737
Zebrowski J J and Baranowski R 2003 *Phys. Rev.* E **67** 056216
van Veen L and Liley D T J 2006 *Phys. Rev. Lett.* **97** 208101
[11] Shilnikov L P 1963 *Math. USSR Sb.* **6** 443
[12] Marino F, Marin F, Balle S and Piro O 2007 *Phys. Rev. Lett.* **98** 074104
[13] Koper M T M, Gaspard P and Sluyters J H 1992 *J. Chem. Phys.* **97** 8250
[14] Arecchi F T, Meucci R and Gadomski W 1987 *Phys. Rev. Lett.* **58** 2205
Pisarchik A N, Meucci R and Arecchi F T 2001 *Eur. Phys. J.* D **13** 385
[15] Hennequin D, de Tomasi F, Zambon B and Arimondo E 1988 *Phys. Rev.* A **37** 2243
Dangoisse D, Bekkali A, Papoff F and Glorieux P 1988 *Europhys. Lett.* **6** 335
[16] Eguia M C and Mindlin G B 1999 *Phys. Rev.* E **61** 6490
[17] Chow W W, Koch S W and Sargent M 1994 *Semiconductor Laser Physics* (Berlin: Springer)
[18] Tang S and Liu J M 2001 *IEEE J. Quantum Electron.* **37** 329
[19] Rogister F, Locquet A, Pieroux D, Sciamanna M, Deparis O, Megret P and Blondel M 2001 *Opt. Lett.* **26** 1486
[20] Saucedo Solorio J M, Sukow D W, Hicks D R and Gavrielides A 2002 *Opt. Commun.* **214** 327
[21] Deng B 2004 *Chaos* **14** 1083
[22] Hirsch M W and Smale S 1974 *Differential Equations, Dynamic Systems and Linear Algebra* (New York: Academic)